

## Article

# Optical and Physicochemical Characterizations of a Cellulosic/CdSe-QDs@S-DAB<sub>5</sub> Film

Manuel Algarra <sup>1,\*</sup> , Ana L. Cuevas <sup>2</sup> , Ma Valle Martínez de Yuso <sup>3</sup>, Rocío Romero <sup>2</sup>, Beatriz Alonso <sup>4</sup> , Carmen M. Casado <sup>4</sup> and Juana Benavente <sup>5,\*</sup>

<sup>1</sup> INAMAT2-Institute for Advanced Materials and Mathematics, Departamento de Ciencias, Universidad Pública de Navarra, Campus de Arrosadía, 31006 Pamplona, Spain

<sup>2</sup> Unidad de Nanotecnología, Centro de Supercomputación y Bioinnovación, Servicios Centrales de Investigación, Universidad de Málaga, 29071 Málaga, Spain; analaura.cuevas@uma.es (A.L.C.); rociorp@uma.es (R.R.)

<sup>3</sup> X-ray Photoelectron Spectroscopy Lab., Central Service to Support Research Building (SCAI), Universidad de Málaga, 29071 Málaga, Spain; mvyuso@uma.es

<sup>4</sup> Departamento de Química Inorgánica, Universidad Autónoma de Madrid, Cantoblanco, 28049 Madrid, Spain; beatriz.alonso@uam.es (B.A.); carmenm.casado@uam.es (C.M.C.)

<sup>5</sup> Departamento de Física Aplicada I, Facultad de Ciencias, Universidad de Málaga, 29071 Málaga, Spain

\* Correspondence: manuel.algarra@unavarra.es (M.A.); j\_benavente@uma.es (J.B.); Tel.: +34-948-169822 (M.A.)

**Abstract:** CdSe quantum dots nanoparticles were coated with the thiolated (DiAminoButane based dendrimer) DAB dendrimer of fifth generation (S-DAB<sub>5</sub>) and embedded in a highly hydrophilic regenerated cellulose (RC) film by simple dip-coating method (immersion in QD-dendrimer aqueous solution) as a way to get a flexible nano-engineered film (RC-4/CdSe-QDs@S-DAB<sub>5</sub>) with high transparency and photoluminescence properties for different applications. Optical changes in the RC film associated with QDs inclusion were determined by spectroscopic ellipsometry (SE) measurements, which provide information on changes caused in the refraction index and the extinction coefficients of the film, as well as by light transmittance/reflectance curves and photoluminescence (PL) spectra. Impedance spectroscopy (IS) and other typical physicochemical techniques for material characterization (TEM, SEM and XPS) have also been used in order to have more complete information on film characteristics. A comparison of RC-4/CdSe-QDs@S-DAB<sub>5</sub> film optical characteristics with those exhibited by other RC-modified films depending on the type of dendrimer was also carried out.

**Keywords:** CdSe quantum dots; dendrimers; regenerated cellulose modified film; optical properties



**Citation:** Algarra, M.; Cuevas, A.L.; Yuso, M.V.M.d.; Romero, R.; Alonso, B.; Casado, C.M.; Benavente, J. Optical and Physicochemical Characterizations of a Cellulosic/CdSe-QDs@S-DAB<sub>5</sub> Film. *Nanomaterials* **2022**, *12*, 484. <https://doi.org/10.3390/nano12030484>

Academic Editor:  
Vladimir Chaldyshev

Received: 10 December 2021

Accepted: 26 January 2022

Published: 29 January 2022

**Publisher's Note:** MDPI stays neutral with regard to jurisdictional claims in published maps and institutional affiliations.



**Copyright:** © 2022 by the authors. Licensee MDPI, Basel, Switzerland. This article is an open access article distributed under the terms and conditions of the Creative Commons Attribution (CC BY) license (<https://creativecommons.org/licenses/by/4.0/>).

## 1. Introduction

Colloidal quantum dot (QD) nanoparticles are semiconductor nanocrystals, with a core-shell structure and a diameter ranging ideally between 2 nm and 10 nm, which display unique electronic and optical properties (between bulk semiconductors and discrete molecules) based on both size and chemical composition [1–5]. QDs can emit light at wavelengths ranging from the UV to the IR, a photon emission at a longer wavelength than the one absorbed (electron-hole recombination process) [6]. Their properties include highest photostability, high extinction coefficient and brightness, magnetic, thermal and antibacterial characteristics as well as small size, this latter being a great advantage over other nanoparticles (NPs) used for multifunctional probes (polymeric or silica NPs), due to their large surface area [7].

In fact, QDs are nowadays of significant interest in different nanotechnology fields such as biomedical, electronics and optoelectronic devices due to their pure color emission, wide color gamut and high quantum efficiency [8]. Moreover, QDs also exhibit narrow band gap, sharp emission, and excellent spectral properties [9–11], but they are unprotected from external agents (oxidation, water, heat, or harsh environments) which significantly limit their long-term stability [12–14]. In this context, the inclusion of QDs

into transparent polymeric matrices has been considered as a way of reducing fluorescence quenching and improving QDs stability [15]. Different QDs (CdSe, CdTe, CdSe/ZnS, carbon, nitrogen-doped carbon, graphene) and support matrices (poly(methyl methacrylate), polyamide, transparent wood, cellulose, etc.) for electronic devices, solar concentrators, white light-emitting diodes, sensors or agriculture (sunlight conversion films) have already been reported [16–25]. Among them, regenerated cellulose (RC), a flexible, transparent, biodegradable and low-cost material, exhibits appropriated characteristics for QDs modification [26–29]. Moreover, the high hydrophilic character of RC films has already permitted the inclusion of different nanoparticles by depth-coating in water solutions of desired NPs, a method that does not require complex processes [30–32]. In this regard, QDs coverage with dendrimers, such as thiol DAB, seems to increase photoluminescence intensity, reduce their possible toxicity and favor their link with the cellulose chains, as it was already obtained in our previous works [33–35].

Dendrimers are macromolecules synthesized with very high precision (monodispersed macromolecules) following a bottom-up approach, which allows an almost total control in both size and surface properties, making them an attractive platform for very diverse applications such as imaging or detecting agents (dye molecule), targeting components, radioligands or pharmaceutically active compounds [36,37]. In this context, it is known that polyamidoamine dendrimers (PAMAMs) can adsorb small molecules in a non-covalent way, which helps to the controlled delivery of fluorescent systems [38]. In fact, the binding of dendrimers to nanoparticles, more specifically to QDs, seems to preserve them from environmental effects, improving their emissive properties both at energy and intensity levels [39,40]. Dendrimers are characterized by being built by segments of molecules giving rise to different generations, that is, macromolecules of different size; those of small size are the best acting as stabilizing agents for NPs coverage, but when they exceed generation 5 (very branched structures) can be more effectively incorporated to the NPs surface due to the great presence of carbonyl and amine functional groups, which facilitate the adsorption of NPs [41,42].

The objective of this work is to obtain a flexible, highly transparent and luminescent film with potential use in optoelectronic devices. For that purpose, CdSe QDs covered by a DAB dendrimer generation 5 with thiol endings functional organic groups (S-DAB<sub>5</sub>) were included in a highly swollen regenerated cellulose film by simple depth-coating process (RC-4/CdSe-QDs@S-DAB<sub>5</sub> film). Basic information on surface and bulk modification of the QDs nano-engineered film was obtained by FE-SEM and TEM microscopy, XPS and impedance spectroscopy techniques, while their optical properties were determined by photoluminescence spectra as well as by light transmittance/reflectance and spectroscopic ellipsometry measurements. These latter results provide information on film characteristic optical parameters (refraction index and extinction coefficient) and anisotropy due to CdSe-QDs@S-DAB<sub>5</sub> NPs inclusion in the RC support. This kind of hybrid system with tailoring optical parameters can be of interest in different applications (photovoltaic devices, light-emitting devices, etc.) [19,23–25].

## 2. Materials and Methods

### 2.1. Preparation of CdSe QDs and Thiolated DAB Generation 5 Dendrimer

The synthesis of CdSe-QDs was performed following the procedure previously indicated in reference [43]. Briefly, CdCl<sub>2</sub> (0.2 mM) was dissolved in H<sub>2</sub>O (50 mL) and, after total dissolution, 3-mercaptopropyl acid (2.2 mM) was added and left overnight to ensure the coating process, previously to the addition of Se, which was prepared as NaHSe to avoid further oxidation process. CdSe QDs powders with strong fluorescent under UV radiation were obtained after the purification step with EtOH/H<sub>2</sub>O dissolutions.

Thiolate DAB dendrimer generation 5 (S-DAB<sub>5</sub>) was prepared according to the procedure previously indicated in [44]; 3-mercaptopropanyl-N-hydroxysuccinimide ester, dendritic polyamine DAB-AM and triethylamine in CH<sub>2</sub>Cl<sub>2</sub> was used for S-DAB<sub>5</sub> dendrimer synthesis; the obtained dendrimer (formulae: (NHCH<sub>2</sub>CH<sub>2</sub>SH)<sub>64</sub>, mass: 12,808.1323

u.a.m and size of around 6.6 nm) is soluble in aqueous solutions but insoluble in organic solvents. Figure 1a shows a schematic of the S-DAB<sub>5</sub> dendrimer, while Figure 1b shows the CdSe-QDs@S-DAB<sub>5</sub> nanoparticles

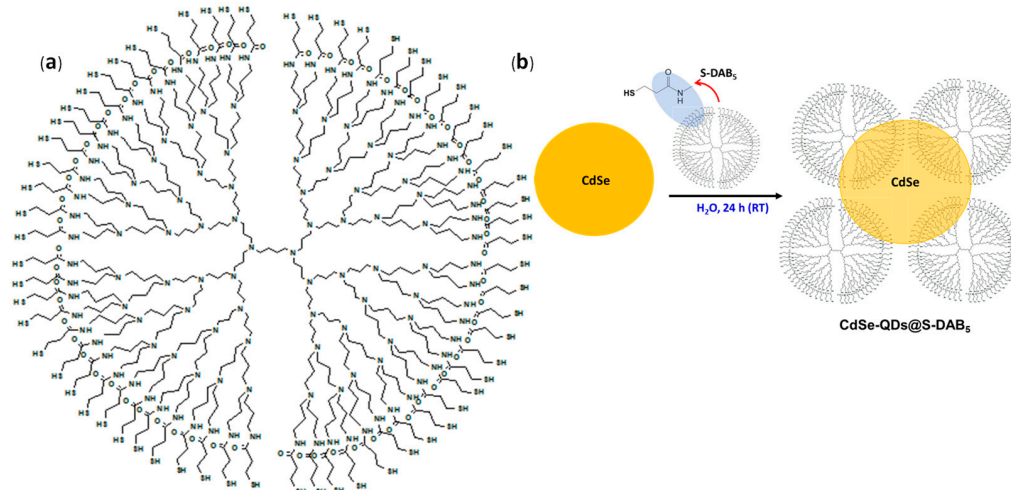


**Figure 1.** Scheme (a) S-DAB<sub>5</sub> and (b) CdSe-QDs nanoparticles coated by S-DAB<sub>5</sub> dendrimer (ChemWindow Chemical Structure Drawing Software from Wiley).

## 2.2. Preparation of the Cellulosic Films Modified with CdSe-QDs@ S-DAB<sub>5</sub> Nanoparticles

A highly swelling (>80%), elastic, and transparent film of regenerated cellulose (RC) from Cellophane Española S.A. (Burgos, Spain was selected for easy inclusion of CdSe-QDs@S-DAB<sub>5</sub> by depth-coating method) [43]. Pieces of the RC-4 film were immersed in an aqueous solution of CdSe-QDs@S-DAB<sub>5</sub> for 2 h at room temperature, then they were taken off and their surfaces gently dried with paper. These samples will be named RC-4/CdSe-QDs@S-DAB<sub>5</sub>, and a scheme of this flexible and easily handle film is shown in Figure 2.

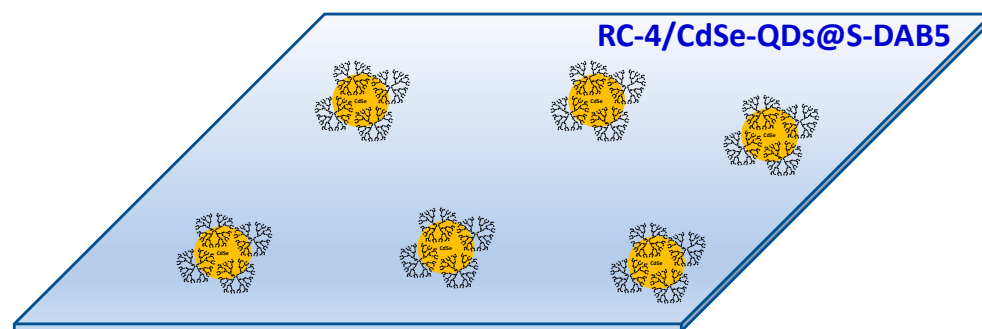


**Figure 2.** Scheme of the RC-4/CdSe-QDs@S-DAB<sub>5</sub> film.

## 2.3. Surface Analysis: FE-SEM Microscopy and XPS Spectroscopy

The surface morphology of the cellulosic film coated with CdSe-G<sub>5</sub> QDs nanoparticles was analyzed using an FEI Talos F200X field-emission scanning electron microscope (FE-SEM) with a double beam (Helios Nanolab 650 de FEI Company, Oxford, UK). Surface chemical characterization of the studied film was carried out by X-ray photoelectron spectroscopy (XPS, Physical Electronics ULVAC-PHI Lake Drive East, Chanhassen, MN, USA). XPS spectra were recorded with a Physical Electronics PHI 5700 spectrometer with X-ray MgK $\alpha$  radiation as the excitation source (300 W, 15 kV, 1253.6 eV). High-resolution spectra were recorded at two take off angles, 45° (standard analysis angle) and 70°, by a concentric hemispherical analyzer operating in the constant pass energy mode at 29.35 eV and using a diameter analysis area of 720  $\mu$ m. The residual pressure in the analysis chamber was maintained below 10<sup>-9</sup> Torr during data acquisition. Accurate  $\pm$ 0.1 eV

binding energies were determined with respect to the position of the adventitious C 1s peak at 284.8 eV. A PHI ACCESS ESCA-V6.0F software package was used for acquisition and data analysis. Atomic concentration percentages (A.C. %) of the sample elements were determined after subtraction of a Shirley-type background considering the corresponding area sensitivity factor for the different measured spectral regions [45].

#### 2.4. Optical Characterization

An Edinburgh Instruments FLS920 (Livingston, UK), equipped with a Xe lamp (450 W) as the excitation source and monochromatic LEDs (PicoQuant PLS), controlled by a PDL880-B system, was used for steady-state fluorescence measurements.

Transmittance/reflection measurements were performed with a Varian Cary 5000 spectrophotometer (Agilent Technologies, Santa Clara, CA, USA) provided with an integrating sphere of Spectralon for wavelength ranging between 250–2000 nm.

Spectroscopic Ellipsometry (SE) measurements were carried out with a spectroscopic ellipsometer (Sopra-Semilab GES-5E) using wavelengths in the range from 200 nm to 1000 nm after striped the back surface of the sample for reduction of interference fringes associated with multiple light reflections at the back interface (see Supplementary Figure S1). WinElli software v. 2.2 (Sopra-Semilab, Paris, France) was used for data fit. SE is a non-destructive technique that allows the determination of optical/morphological parameters of inorganic and polymeric thin films (refraction index, extinction coefficient or thickness) [46–48]. Two characteristic parameters, angles  $\Psi$  and  $\Delta$ , are measured to determine changes associated to film surface or bulk phase [46,49], which are related with differential changes in amplitude and phase between the incident and reflected light waves (through the Fresnel reflection coefficients ratio of polarized light) by [46]:

$$\tan(\Psi)e^{i\Delta} = r_p/r_s \quad (1)$$

where  $r_s$  and  $r_p$  indicate the amount of light in perpendicular (s) and parallel (p) planes, as it is schematically shown in Figure 3. Because SE is based on the ratio of two measured values, it is very accurate and reproducible, and no standard sample is required [46].

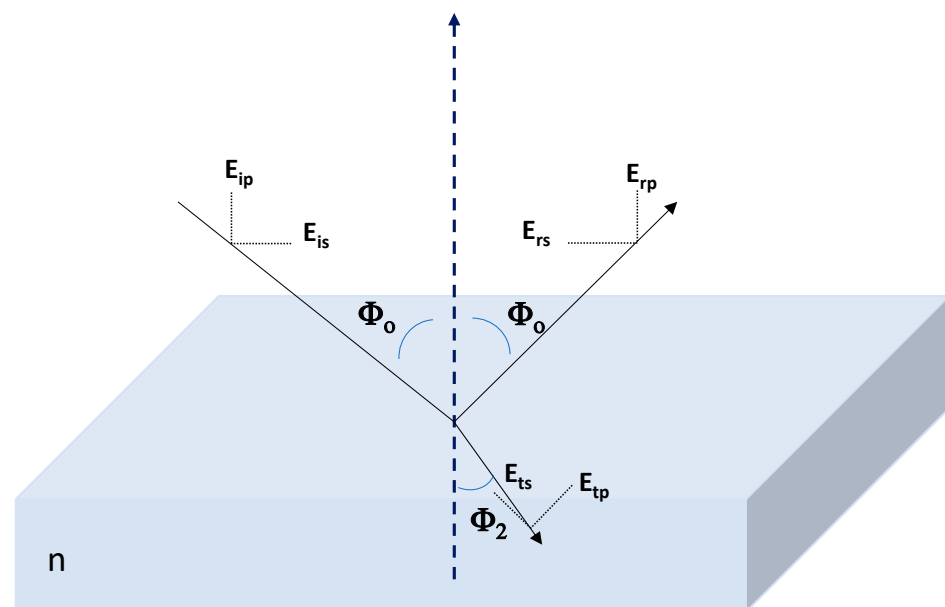


**Figure 3.** Scheme of spectroscopy ellipsometry measurement for a homogeneous sample.  $\Phi_0$  incident angle;  $\Phi_2$ : refraction angle.  $E_{is}$ : perpendicular component of the incident electric field;  $E_{ip}$ : parallel component of the incident electric field;  $E_{rs}$ : perpendicular component of the reflected electric field;  $E_{rp}$ : parallel component of the reflected electric field;  $E_{ts}$ : perpendicular component of the refracted electric field;  $E_{tp}$ : parallel component of the refracted electric field. Sample refraction index:  $n$ .

SE measurements were performed at three different incident angles ( $\Phi_0 = 65^\circ, 70^\circ$  and  $75^\circ$ ) since it can also give information on sample homogeneity, the presence of surface impurities and roughness [49,50].

### 2.5. Impedance Spectroscopy Measurements

Impedance spectroscopy (IS) measurements were performed with dry samples in an electrode/sample/electrode test cell [51]. The electrodes were connected to an Impedance Analyzer (Solartron 1260, Solartron Analytical, Wokingham, UK) and measurements were recorded for 100 data points with frequency ( $f$ ) ranging between 10 Hz and  $10^7$  Hz, at a maximum voltage of 0.01 V. The impedance,  $Z$ , is a complex number,  $Z = Z_{\text{real}} + j Z_{\text{img}}$ , which can be separated into real and imaginary parts by algebra rules. Electrical parameters (resistance (R) and capacitance (C)) can be determined by analyzing the impedance plot ( $Z_{\text{real}}$  versus  $-Z_{\text{img}}$ ) by considering equivalent circuits. The simplest case, for homogeneous systems, corresponds to a semi-circle and it is due to a parallel association of resistance (R) and capacitor (C) [46], which are related to  $Z_{\text{real}}$  and  $Z_{\text{img}}$  by the following expressions:

$$Z_{\text{real}} = (R/[1 + (\omega RC)^2]) \quad (2)$$

$$Z_{\text{img}} = - (\omega R^2 C/[1 + (\omega RC)^2]) \quad (3)$$

where  $\omega$  represents the angular frequency ( $\omega = 2\pi f$ ). However, complex systems usually present distribution of relaxation times and the resulting plot is a depressed semi-circle, which is associated with a non-ideal capacitor or constant phase element (CPE), and its impedance is expressed by [52]:  $Q(\omega) = Y_0(j\omega)^{-m}$ , where  $Y_0$  represents the admittance and  $m$  is an experimental parameter ( $0 \leq m \leq 1$ ) and in these cases an equivalent capacitance ( $C^{\text{eq}}$ ) can be determined. This kind of analysis allows us to determine the presence/effect of different polymer-modifying elements [53,54].

## 3. Results and Discussion

### 3.1. Surface and Bulk Analysis

Figure 4 shows the FE-SEM image of the RC-4/CdSe QDs-DAB<sub>5</sub> film, where the presence of the CdSe QDs@S-DAB<sub>5</sub> nanoparticles on the surface of the RC-4 film is clearly observed, while the EDAX analysis gives the following values, in atomic (%): C (29.5%); O (37.3%); S (21.4%); Cd (1.9%) and Se (0.2%). In addition, TEM images of the synthesized nanoparticles (in solution) and the EDAX analysis (performed with a Philips CM 200 microscope) [43] are presented as Supplementary Materials (Figure S2 and Figure S3, respectively).

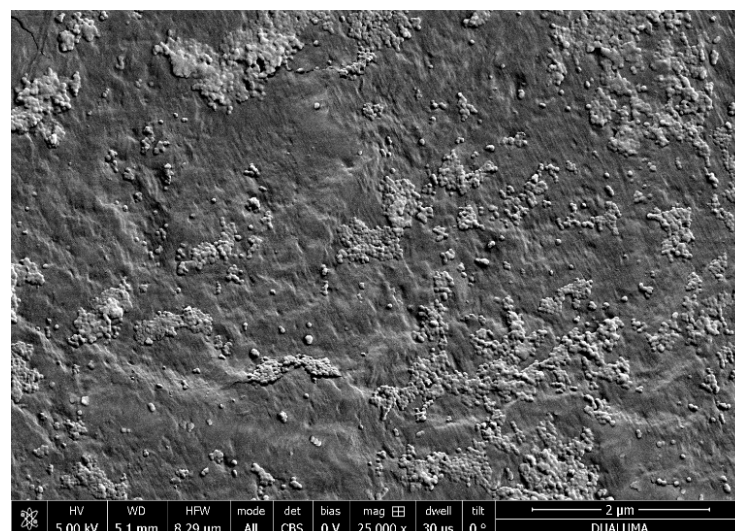
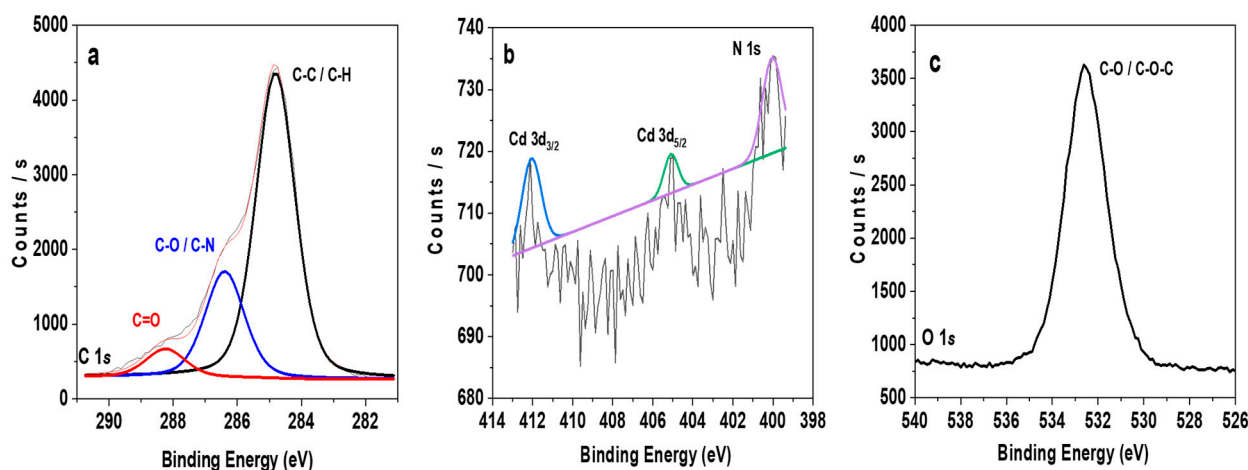


Figure 4. FE-SEM images of RC-4/CdSe-QDs@S-DAB<sub>5</sub> film.

On the other hand, when the surface analysis is carried out by XPS, it is possible to detect the presence of other atoms such as nitrogen, by the N 1s signal from the dendritic structure. Here the surface chemical concentrations (in A.C.%) at the standard analysis angle ( $45^\circ$ ) are: C 1s (77.5%); O 1s (20.5%); N 1s (0.4%); Cd 3d (0.02%) and Se 5d (0.02%); moreover, a slight increase in Cd 3d and Se 5d values (0.03%) was obtained from measurement performed at a higher incident angle ( $70^\circ$ ), which corresponds to deeper analysis, which seems to confirm the presence of CdSe QDs-DAB<sub>5</sub> into the film structure (A.C. % of the different elements at  $70^\circ$  incident angle are indicated in Supplementary Information (Table S1)).

The XPS study of the surface provides the chemical oxidation state of the characteristic QDs ions (Figure 5). The analysis of the C 1s reveals the presence of three main contributions assigned to: (i) adventitious carbon ( $sp^2$  hybridized carbon) –C–C–/–C–H at 284.8 (69.53%); (ii) –C–OH/–C–N at 286.39 (24.1%) and (iii) –C=O at 288.2 eV (6.5%) functional groups (Figure 5a), related mainly to the presence of dendrimer molecule [55]. On the other hand, the N 1s spectra (Figure 5b) exhibits a major peak at around 400.0 eV and it was attributed to N atoms bonded with  $sp^2$ -hybridized C atoms [56]; Figure 5b also shows the Cd 3d signal from the QDs, at 405.1 and 412.1 eV, assigned to the  $3d_{3/2}$  and  $3d_{5/2}$  orbitals. Figure 5c shows the O 1s signal, a peak at 532.5 eV, assigned to the C–O and C–O–C signal. It should be indicated that the Se signal was not observed due to its low sensitivity factor and dendrimer coverage.



**Figure 5.** XPS core level spectra of RC-4/CdSe QDs-DAB<sub>5</sub> film: (a) C 1s; (b) Cd 3d and N 1s; (c) O 1s.

Another technique able to give information on bulk material and interface (electrode/sample surface) contributions is impedance spectroscopy (IS). IS is an alternating current (a.c.) technique commonly used for electrical characterization of homogeneous and heterogeneous materials as well as for composite systems (such as electrolyte/sample commonly named Electrochemical Impedance Spectroscopy or EIS) using equivalent circuits as models [53,54,57,58]. IS provides quantitative and/or qualitative information related to charge movement/adsorption for the analyzed samples by means of the electrical resistance or capacitance (equivalent capacitance for non-homogeneous systems,  $C^{eq} = (RY_0)^{(1/m)}/R$  [52]) respectively, which can be significantly affected by the structure of the analyzed system and material characteristics. Figure 6a shows the Nyquist plot ( $Z_{real}$  vs.  $-Z_{img}$ ) obtained for dry samples of the original RC-4 film and the modified RC-4/CdSe-QDs@S-DAB<sub>5</sub> one, where differences in both bulk sample and electrode/sample interface can be observed. For comparison reason, the Nyquist plot for another nano-engineered film, RC-4/CdSe-QDs@S-DAB<sub>2</sub>, modified with CdSe QDs covered by S-DAB<sub>2</sub> dendrimer (formula and mass:  $NHCH_2CH_2SH$ )<sub>8</sub> and 1478.3187 u.m.a.) is shown in Figure 6b, and in this case, practically no differences were obtained for the electrode/sample region, although slight differences in the bulk films contribution can be observed. Figure 6c,d show the Bode plots ( $Z_{real}$  vs.  $f$  and  $-Z_{img}$  vs.  $f$ , respectively) which permit seeing in a clearer way the

differences between RC-4 and RC-4/CdSe-QDs@S-DAB<sub>5</sub> films, where the slight shift to lower frequency obtained for this latter film is an indication of its more compact structure associated with the nanoparticles inclusion.

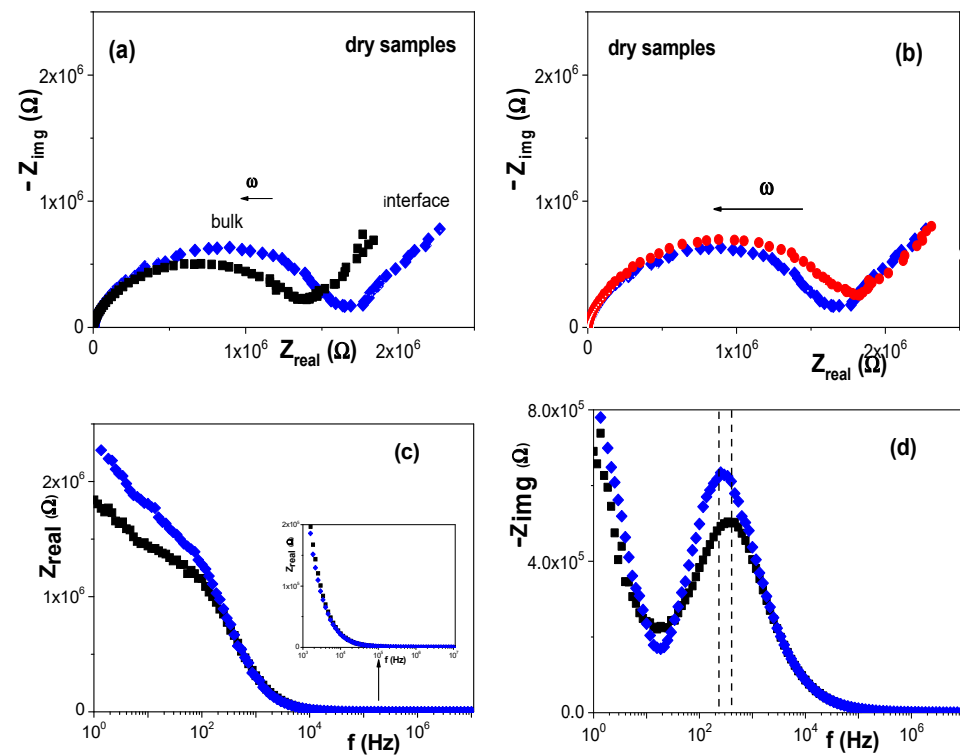


**Figure 6.** Impedance plots: (a) and (b) Nyquist plot ( $Z_{\text{real}}$  vs.  $-Z_{\text{img}}$ ); (c)  $Z_{\text{real}}$  as a function of frequency; (d)  $-Z_{\text{img}}$  as a function of frequency. (■) RC-4 film; (◆) RC-4/CdSe-QDs@S-DAB<sub>5</sub> film; (●) RC-4/CdSe-QDs@S-DAB<sub>2</sub> film.

The fit of the two slightly depressed semicircles shown in Figure 6a by a non-linear program allows us the estimation of the electrical resistance (R) and equivalent capacitance ( $C^{\text{eq}}$ ) of the films, which permits the determination of their electrical conductivity ( $\sigma = d/S \cdot R$ ) and dielectric constant ( $\epsilon = C \cdot d/S$ ), where d and S represent the thickness and surface of the films, respectively. The values obtained for the RC-4/CdSe-QDs@S-DAB<sub>5</sub> film are:  $\sigma = 3.1 \times 10^{-7} (\Omega \cdot \text{m})^{-1}$  and  $\epsilon = 8.1$ , which represent a reduction of around 18% in the conductivity and an increase of 7% in the dielectric constant with respect to the support film. Therefore, IS results seem to confirm the presence of CdSe-QDs@S-DAB<sub>5</sub> into the structure of the cellulosic film as well as on its surface.

### 3.2. Optical Analysis

Optical characterization techniques, photoluminescence (PL), light transmission and spectroscopic ellipsometry (SE) are of great interest in the analysis of thin films due to their non-invasive/non-destructive character, providing important characteristics of the analyzed samples.

One of the most significant properties of CdSe QDs is their fluorescent emission, with a maximum intensity of 534 nm; consequently, the luminescence character of the RC-4/CdSe-QDs@S-DAB<sub>5</sub> film shown in Figure 7, obtained at an excitation source of 475 nm, was expected. The emission spectra of the QDs-dendrimer modified film show an intensity maximum at 536 nm and exhibits higher intensity than that presented by the CdSe QDs. This fact is associated with the presence of the dendrimer on the surface of the QDs, since the thiol terminal functional groups increase the QDs emission process, as was already indicated in a previous study [59], but they do not change the emission wavelength.

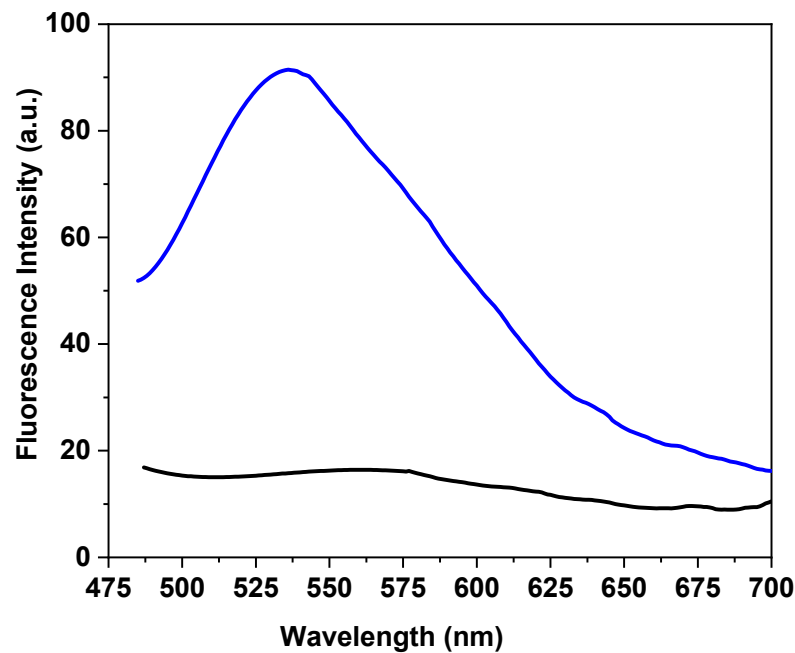


Figure 7. Comparison of the fluorescence spectra for the RC-4/CdSe-QDs@S-DAB<sub>5</sub> (blue line) and RC-4 (black line) films excited at 475 nm.

Spectroscopic ellipsometry (SE) results are presented in Figure 8. In particular, Figure 8a,b show a comparison of the wavelength dependence of the experimental parameters,  $\tan(\Psi)$  and  $\cos(\Delta)$ , measured at different light incident angles ( $\Phi_0 = 65^\circ, 70^\circ$  or  $75^\circ$ ) for the RC-4/CdSe-QDs@S-DAB<sub>5</sub> film and the RC-4 support, where differences depending on both incident angle and film can be observed. Optical characteristic parameters such as the refractive index ( $n$ ) and the extinction coefficient ( $k$ ) can be determined from SE measurements using the ellipsometer software, and their dependence on wavelength at the different light incident angles is shown in Figure 8c,d, respectively, for both films.

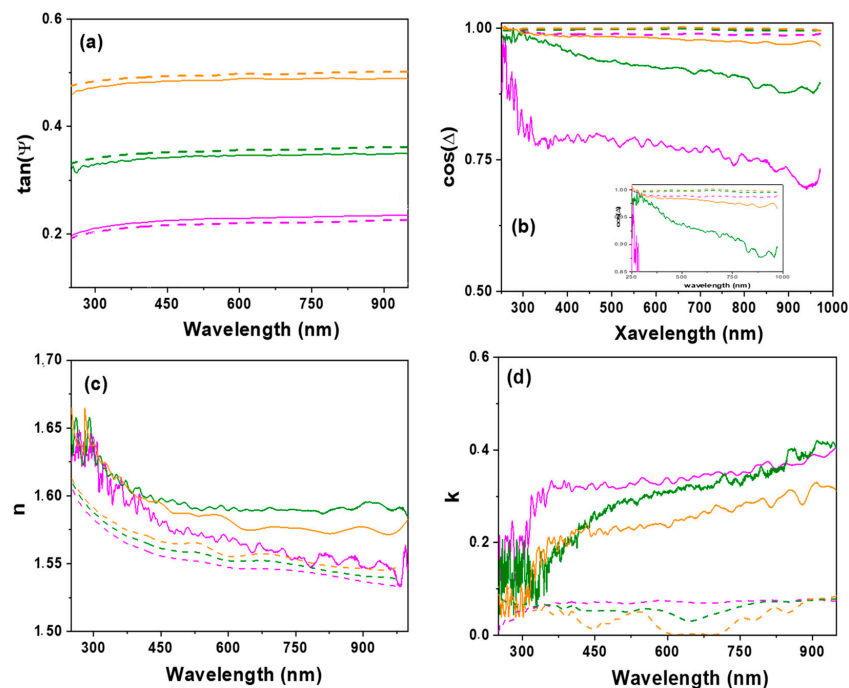
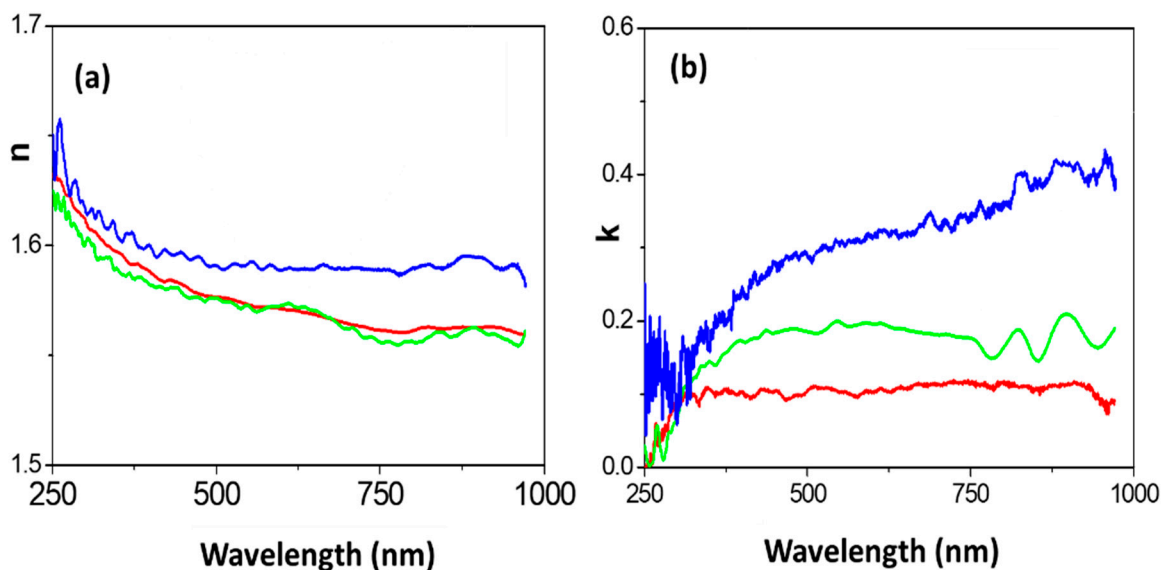


Figure 8. Wavelength dependence of: (a)  $\tan(\Psi)$ ; (b)  $\cos(\Delta)$ ; (c) refractive index; (d) extinction coefficient, for the RC-4 support (dashed lines) and the RC-4/CdSe-QDs@S-DAB<sub>5</sub> film (solid lines) determined at different light incident angles:  $65^\circ$  (magenta line),  $70^\circ$  (green line) and  $75^\circ$  (orange line).

As it can be observed in Figure 8c rather similar values for both refraction index and extinction coefficient were obtained at the different light incident angles for the RC-4 support, which is an indication of film smooth surface and homogeneity, and the small differences are attributed to surface impurities associated to environmental contamination; the following average values were determined:  $\langle n \rangle = 1.56 \pm 0.03$  and  $\langle k \rangle = 0.06 \pm 0.03$ , which do not differ significantly from those reported for regenerated cellulose (1.48) and other polymers (between 1.53 and 1.58) measured at a unique wavelength of 589 nm [60], and zero in the case of extinction coefficient (no light absorption). However, higher values variability depending on the light incident angle was obtained for the RC-4/CdSe-QDs@S-DAB<sub>5</sub> film, which is attributed to sample inhomogeneity caused by inclusion of the CdSe-QDs@S-DAB<sub>5</sub> nanoparticles, as well as the surface roughness associated to CdSe QDs presence already established by SEM images. The following average values for the refraction index were estimated:  $\langle n(65^\circ) \rangle = 1.58 \pm 0.05$ ,  $\langle n(70^\circ) \rangle = 1.62 \pm 0.03$  and  $\langle n(75^\circ) \rangle = 1.59 \pm 0.03$ ; in the case of the extinction coefficient:  $\langle k(65^\circ) \rangle = 0.32 \pm 0.03$ ,  $\langle k(70^\circ) \rangle = 0.27 \pm 0.09$  and  $\langle k(75^\circ) \rangle = 0.22 \pm 0.11$ , indicating higher light absorption by the modified film. Consequently, the increase of  $n$  and  $k$  values determined for the RC-4/CdSe-QDs@S-DAB<sub>5</sub> film with respect to the RC-4 support is an indication of CdSe QDs contribution in the optical behavior of the modified film (reported values for CdSe refractive index range between 2.35 and 2.64 [61]).

The effect of the type of QDs (bare silicon dots, carbon dots, or nitrogen-doped carbon dots) on optical characteristics of the RC-QDs modified films was already studied in a previous paper [28] by comparing wavelength dependence of  $n$  and  $k$  parameters, and differences in both curve shape and values depending on the selected QDs nanoparticles were obtained. Therefore, the effect on optical parameters associated with dendrimers coverage of the CdSe QDs was considered in this work; then, three different generations of S-DAB dendrimers (2, 3 and 5 generations) were considered: (i) the RC-4/CdSe-QDs@S-DAB<sub>5</sub> film, (ii) the RC-4/CdSe-QDs@S-DAB<sub>2</sub> film (CdSe QDs covered with the generation 2 S-DAB dendrimer indicated above), and (iii) the RC-4/CdSe-QDs@S-DAB<sub>3</sub> film (CdSe QDs covered with the generation 3 dendrimer; formulae and mass:  $(\text{NHCH}_2\text{CH}_2\text{SH})_{16}$  and 3096.8635 u.a.m.), and the wavelength dependence of  $n$  and  $k$  for these three RC-4/CdSe-QDs@S-DAB<sub>x</sub> modified films, at a light incident angle of  $70^\circ$ , is shown in Figure 9. As it can be observed,  $n$  and  $k$  parameters determined for the three films exhibit a similar type of wavelength dependence, but differences in the corresponding values depending on dendrimer generation were obtained, with the following sequence: RC-4/CdSe-QDs@S-DAB<sub>5</sub> film > RC-4/CdSe-QDs@S-DAB<sub>3</sub> film > RC-4/CdSe-QDs@S-DAB<sub>2</sub>, being this fact more significant for the extinction coefficient. Consequently, the choice of both the type of QDs and their coating allows us to obtain films with differentiated optical properties. On the other hand, it should be indicated that SE results also provide information on the real and the imaginary parts of the dielectric constant ( $\epsilon_r$  and  $\epsilon_i$ , respectively) considering that  $\epsilon = (n + i k)^2$  [46], which could be of interest in some applications.

The effect of CdSe-QDs inclusion on light transmission and reflection characteristics of the support film was also investigated. Figure 10a shows the transmittance spectra for the RC-4 and the RC-4/CdSe-QDs@S-DAB<sub>5</sub> films, and practically no effect due to the presence of the nanoparticles is observed in the visible region, but slight differences in the near-infrared (NIR) region were obtained (1% average reduction); this fact seems to be related to the dendrimer coverage since similar dependence for the whole wavelength range was obtained for the RC-4/CdSe-QDs@S-DAB<sub>5</sub> and the RC-4/CdSe-QDs@S-DAB<sub>3</sub> films (see the insert in Figure 10a). High transmittance values are of interest for optical applications; in fact, the value obtained (>90%) is like that reported for carboxymethyl cellulose films modified with carbon dots with application in agriculture (sunlight conversion) [21].



**Figure 9.** Wavelength dependence of refractive index (a) and extinction coefficient (b) for: RC-4/CdSe-QDs@S-DAB<sub>5</sub> film (blue line), RC-4/CdSe-QDs@S-DAB<sub>3</sub> film (green line) and RC-4/CdSe-QDs@S-DAB<sub>2</sub> film (red line) at 70° light incident angle.

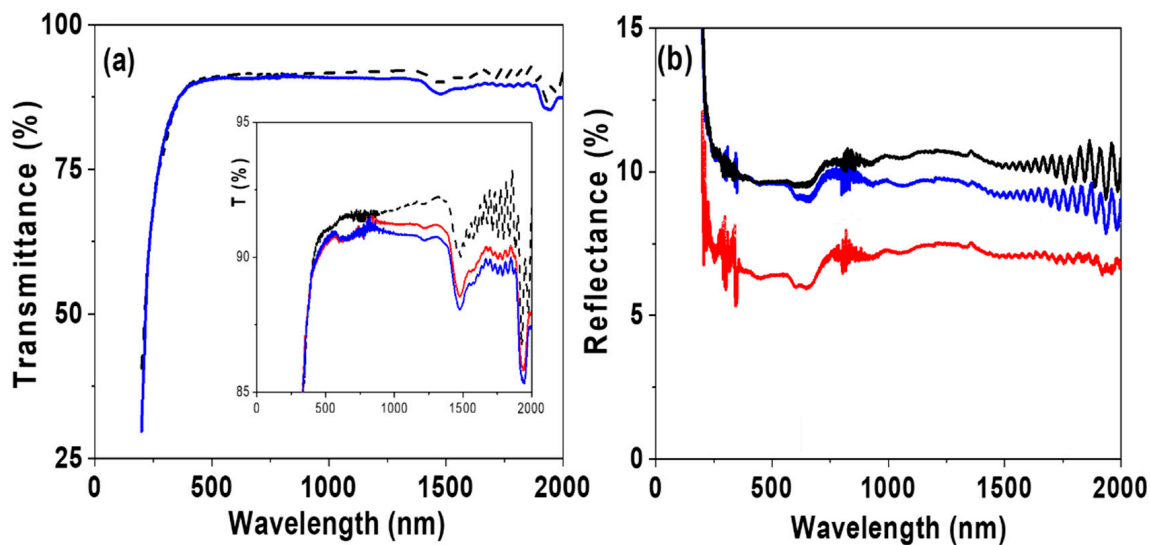


**Figure 10.** Wavelength dependence of: (a) light transmittance and (b) light reflection. RC-4 film (black line), RC-4/CdSe-QDs@S-DAB<sub>5</sub> film (blue line) and RC-4/CdSe-QDs@S-DAB<sub>3</sub> film (green line).

The comparison of light reflectance spectra obtained for the RC-4 and the RC-4/CdSe-QDs@S-DAB<sub>5</sub> films presented in Figure 10b also shows similar dependence, but an average reflectance % reduction in the NIR region of ~5% due to QDs inclusion. However, the type of dendrimer seems to affect light reflection since a more significant reduction (around 20% for the whole range of wavelength) was obtained for the RC-4/CdSe-QDs@S-DAB<sub>3</sub> film.

#### 4. Conclusions

A photoluminescence film was obtained by the inclusion of CdSe QDs covered by thiolate DAB<sub>5</sub> dendrimer nanoparticles (CdSe-QDs@S-DAB<sub>5</sub>) into a highly swollen and elastic regenerated cellulose (RC) film support by depth-coating into an aqueous solution of these nanoparticles. The nano-engineering RC-4/CdSe-QDs@S-DAB<sub>5</sub> film exhibits modified optical characteristics when compared with the RC-4 support, with a significant increase in the values of the extinction coefficient but only around 4% in the refractive index. Moreover, the influence of the cover-dendrimer generation (S-DAB<sub>2</sub>, S-DAB<sub>3</sub> or S-DAB<sub>5</sub>)

on  $n$  and  $k$  parameters was also demonstrated, indicating that both the types of QDs and the coating (in case) influence both optical parameters. The RC-4/CdSe-QDs@S-DAB<sub>5</sub> film also shows very high transmittance (>90%), with only small changes at the near-infrared region for both light transmission and reflection (around 3%), when compared with the support RC-4 film, and only small changes associated with the dendrimer generation were obtained.

**Supplementary Materials:** The following are available online at <https://www.mdpi.com/article/10.3390/nano12030484/s1>, Figure S1: Comparison of wavelength dependence ( $\Psi$ ) for a non-stripped RC-4 sample (dashed line) and a striped RC-4 sample (dense line). Figure S2. TEM images of CdSe-QDs@S-DAB<sub>5</sub> nanoparticles in solution. Figure S3. EDAX spectra of the CdSe-QDs@S-DAB<sub>5</sub> nanoparticles. Table S1. Atomic concentration percentages (%) of the elements observed on the surface of the RC-4/CdSe@S-DAB<sub>5</sub> film at 70° take off angle.

**Author Contributions:** Conceptualization, M.A. and J.B.; methodology, A.L.C., R.R., B.A. and C.M.C.; formal analysis, M.A. and J.B.; investigation, M.A., A.L.C., R.R., M.V.M.d.Y., B.A. and J.B.; resources, M.A., A.L.C., R.R., B.A. and J.B.; writing—original draft preparation, M.A. and J.B.; writing—review and editing, M.A. and J.B.; supervision, M.A. and J.B. All authors have read and agreed to the published version of the manuscript.

**Funding:** This research received no external funding.

**Institutional Review Board Statement:** Not applicable.

**Informed Consent Statement:** Not applicable.

**Data Availability Statement:** Not applicable.

**Conflicts of Interest:** The authors declare no conflict of interest.

## References

1. Ekimov, A.; Onushchenko, A.A. Quantum size effect in the optical spectra of semiconductor microcrystals. *Sov. Phys. Semicond.* **1982**, *16*, 775–778. [[CrossRef](#)]
2. Murray, C.B.; Norris, D.J.; Bawendi, M.G. Synthesis and characterization of nearly monodisperse CdE (E = sulfur, selenium, tellurium) semiconductor nanocrystallites. *J. Am. Chem. Soc.* **1993**, *115*, 8706–8715. [[CrossRef](#)]
3. Alivisatos, A.P. Semiconductor Clusters, Nanocrystals, and Quantum Dots. *Science* **1996**, *271*, 933–937. [[CrossRef](#)]
4. Bera, D.; Qian, L.; Tseng, T.-K.; Holloway, P.H. Quantum Dots and Their Multimodal Applications: A Review. *Materials* **2010**, *6*, 2260–2345. [[CrossRef](#)]
5. Singh, K.J.; Ahmed, T.; Gautam, P.; Sadhu, A.; Lien, D.-H.; Chen, S.-C.; Chueh, Y.-L.; Kuo, H.-C. Recent Advances in Two-Dimensional Quantum Dots and Their Applications. *Nanomaterials* **2021**, *11*, 1549. [[CrossRef](#)]
6. Efros, A.L.; Brus, L.E. Nanocrystal Quantum Dots: From Discovery to Modern Development. *ACS Nano* **2021**, *15*, 6192–6210. [[CrossRef](#)]
7. Wolfbeis, O.S. An overview of nanoparticles commonly used in fluorescent bioimaging. *Chem. Soc. Rev.* **2015**, *44*, 4743–4768. [[CrossRef](#)]
8. Klimov, V.I. Spectral and Dynamical Properties of Multiexcitons in Semiconductor Nanocrystals. *Annu. Rev. Phys. Chem.* **2007**, *58*, 635–673. [[CrossRef](#)]
9. Amelia, M.; Lincheneau, C.; Silvi, S.; Credi, A. Electrochemical properties of CdSe and CdTe quantum dots. *Chem. Soc. Rev.* **2012**, *41*, 5728–5743. [[CrossRef](#)]
10. Valizadeh, A.; Mikaeili, H.; Samiei, M.; Farkhani, S.M.; Zarghami, N.; Kouhi, M.; Akbarzadeh, A.; Davaran, S. Quantum dots: Synthesis, bioapplications, and toxicity. *Nanoscale Res. Lett.* **2012**, *7*, 48. [[CrossRef](#)]
11. Chizhov, A.; Rumyantseva, M.; Gaskov, A. Light Activation of Nanocrystalline Metal Oxides for Gas Sensing: Principles, Achievements, Challenges. *Nanomaterials* **2021**, *11*, 892. [[CrossRef](#)] [[PubMed](#)]
12. Ko, J.; Jeong, B.G.; Chang, J.H.; Joung, J.F.; Yoon, S.-Y.; Lee, D.C.; Park, S.; Huh, J.; Yang, H.; Bae, W.K.; et al. Chemically resistant and thermally stable quantum dots prepared by shell encapsulation with cross-linkable block copolymer ligands. *NPG Asia Mater.* **2000**, *12*, 19. [[CrossRef](#)]
13. Chen, K.-J.; Chen, H.-C.; Shih, M.-H.; Wang, C.-H.; Kuo, M.-Y.; Yang, Y.-C.; Lin, C.-C.; Kuo, H.-C. The Influence of the Thermal Effect on CdSe/ZnS Quantum Dots in Light-Emitting Diodes. *J. Light. Technol.* **2012**, *30*, 2256–2261. [[CrossRef](#)]
14. Wang, N.; Koh, S.; Jeong, B.G.; Lee, D.; Kim, W.D.; Park, K.; Nam, M.K.; Lee, K.; Kim, Y.; Lee, B.-H.; et al. Highly luminescent silica-coated CdS/CdSe/CdS nanoparticles with strong chemical robustness and excellent thermal stability. *Nanotechnology* **2017**, *28*, 185603. [[CrossRef](#)]

15. Tselikov, G.I.; Timoshenko, V.Y.; Golovan, L.A.; Plenge, J.; Shatalova, A.M.; Shandryuk, G.A.; Kutergina, I.Y.; Merekalov, A.S.; Rühl, E.; Talroze, R.V. Role of the Polymer Matrix on the Photoluminescence of Embedded CdSe Quantum Dots. *ChemPhysChem* **2015**, *16*, 1071–1078. [[CrossRef](#)] [[PubMed](#)]
16. Zhou, M.; Chang, S.; Grover, C.P. Cryptography based on the absorption/emission features of multicolor semiconductor nanocrystal quantum dots. *Opt. Express* **2004**, *12*, 2925–2931. [[CrossRef](#)]
17. Abitbol, T.; Gray, D. CdSe/ZnS QDs Embedded in Cellulose Triacetate Films with Hydrophilic Surfaces. *Chem. Mater.* **2007**, *19*, 4270–4276. [[CrossRef](#)]
18. Shen, L. Biocompatible Polymer/Quantum Dots Hybrid Materials: Current Status and Future Developments. *J. Funct. Biomater.* **2011**, *2*, 355–372. [[CrossRef](#)]
19. Chen, B.; Feng, J. White-Light-Emitting Polymer Composite Film Based on Carbon Dots and Lanthanide Complexes. *J. Phys. Chem. C* **2015**, *119*, 7865–7872. [[CrossRef](#)]
20. Zeng, J.; Yan, L. Metal-free transparent luminescent cellulose films. *Cellulose* **2015**, *22*, 729–736. [[CrossRef](#)]
21. You, Y.; Zhang, H.; Liu, Y.; Lei, B. Transparent sunlight conversion film based on carboxymethyl cellulose and carbon dots. *Carbohydr. Polym.* **2016**, *151*, 245–250. [[CrossRef](#)] [[PubMed](#)]
22. Hill, S.K.E.; Connell, R.; Held, J.; Pedersen, C.; Francis, L.; Hillmayer, M.A.; Ferry, V.E.; Kortshagen, U. Poly(methyl methacrylate) films with high concentrations of silicon quantum dots for visible transparent luminescent solar concentrators. *ACS Appl. Mater. Interfaces* **2020**, *12*, 4572–4578. [[CrossRef](#)] [[PubMed](#)]
23. Zulfajri, M.; Sudewi, S.; Ismulyati, S.; Rasool, A.; Adlim, M.; Huang, G.G. Carbon Dot/Polymer Composites with Various Precursors and Their Sensing Applications: A Review. *Coatings* **2021**, *11*, 1100. [[CrossRef](#)]
24. Danial, W.H.; Md Bahri, N.F.; Abdul Majid, Z. Preparation, Marriage Chemistry and Applications of Graphene Quantum Dots–Nanocellulose Composite: A Brief Review. *Molecules* **2021**, *26*, 6158. [[CrossRef](#)] [[PubMed](#)]
25. Barman, B.K.; Handegård, Ø.S.; Hashimoto, A.; Nagao, T. Carbon Dot/Cellulose-Based Transparent Films for Efficient UV and High-Energy Blue Light Screening. *ACS Sustain. Chem. Eng.* **2021**, *9*, 9879–9890. [[CrossRef](#)]
26. Campos, B.; Gelde, L.; Algarra, M.; da Silva, J.E.; Vázquez, M.; Benavente, J. Characterization of cellulose membranes modified with luminescent silicon quantum dots nanoparticles. *Carbohydr. Polym.* **2016**, *151*, 939–946. [[CrossRef](#)] [[PubMed](#)]
27. Chen, L.; Lai, C.; Marchewka, R.; Berry, R.M.; Tam, K.C. Use of CdS quantum dot-functionalized cellulose nanocrystal films for anti-counterfeiting applications. *Nanoscale* **2016**, *8*, 13288–13296. [[CrossRef](#)]
28. Cuevas, A.; Campos, B.; Romero, R.; Algarra, M.; Vázquez, M.; Benavente, J. Eco-friendly modification of a regenerated cellulose based film by silicon, carbon and N-doped carbon quantum dots. *Carbohydr. Polym.* **2019**, *206*, 238–244. [[CrossRef](#)]
29. Algarra, M.; Cuevas, A.L.; de Yuso, M.V.M.; Benavente, J. Insights into the formation of an emissive CdTe-quantum-dots/cellulose hybrid film. *J. Colloid Interface Sci.* **2020**, *579*, 714–722. [[CrossRef](#)]
30. Ngoensawat, U.; Parnsubsakul, A.; Kaitphaiboonwet, S.; Wutikhun, T.; Sapcharoenkun, C.; Pienpinijtham, P.; Ekgasit, S. Luminescent nanohybrid of ZnO quantum dot and cellulose nanocrystal as anti-counterfeiting ink. *Carbohydr. Polym.* **2021**, *15*, 117864. [[CrossRef](#)]
31. Chinthalapudi, N.; Kommaraju, V.V.D.; Kannan, M.K.; Nalluri, C.B.; Varanasi, S. Composites of cellulose nanofibers and silver nanoparticles for malachite green dye removal from water. *Carbohydr. Polym. Technol. Appl.* **2021**, *2*, 100098. [[CrossRef](#)]
32. Kamel, S.; Khattab, T.A. Recent advances in cellulose supported metal nanoparticles as green and sustainable catalysis for organic synthesis. *Cellulose* **2021**, *28*, 4545–4574. [[CrossRef](#)]
33. Algarra, M.; Campos, B.; Alonso, B.; Miranda, M.; Martínez, Á.M.; Casado, C.; da Silva, J.E. Thiolated DAB dendrimers and CdSe quantum dots nanocomposites for Cd(II) or Pb(II) sensing. *Talanta* **2012**, *88*, 403–407. [[CrossRef](#)] [[PubMed](#)]
34. Esteves da Silva, J.C.G.; Algarra, M.; Campos, B.B. Synthesis and Analytical Applications of Quantum Dots Coated with Different Generations of DAB Dendrimers. In *Advances in Nanocomposites-Synthesis, Characterization and Industrial Applications*; Reddy, B., Ed.; IN-TECH: Rijeka, Croatia, 2011.
35. Algarra, M.; Campos, B.; Miranda, M.; da Silva, J.C.E. CdSe quantum dots capped PAMAM dendrimer nanocomposites for sensing nitroaromatic compounds. *Talanta* **2011**, *83*, 1335–1340. [[CrossRef](#)] [[PubMed](#)]
36. Tomalia, D.A.; Frechet, J.M.J. Discovery of dendrimers and dendritic polymers: A brief historical perspective. *J. Polym. Sci. Part A Polym. Chem.* **2002**, *40*, 2719–2728. [[CrossRef](#)]
37. Lee, C.C.; A Mackay, J.; Frechet, J.; Szoka, F.C. Designing dendrimers for biological applications. *Nat. Biotechnol.* **2005**, *23*, 1517–1526. [[CrossRef](#)] [[PubMed](#)]
38. Sztandera, K.; Gorzkiewicz, M.; Dias Martins, A.S.; Pallante, L.; Zizzi, E.A.; Miceli, M.; Baçal, M.; Pinto Reis, C.; Deriu, M.A.; Klajnert-Maculewicz, B. Noncovalent Interactions with PAMAM and PPI Dendrimers Promote the Cellular Uptake and Photodynamic Activity of Rose Bengal: The Role of the Dendrimer Structure. *J. Med. Chem.* **2021**, *64*, 15758–15771. [[CrossRef](#)] [[PubMed](#)]
39. Bakalova, R.; Zhelev, Z.; Kokuryo, D.; Spasov, L.; Aoki, I. Chemical nature and structure of organic coating of quantum dots is crucial for their application in imaging diagnostics. *Int. J. Nanomed.* **2011**, *6*, 1719–1732. [[CrossRef](#)]
40. Campos, B.B.; Algarra, M.; Alonso, B.; Casado, C.M.; Jiménez, J.J.; Rodríguez-Castellón, E.; da Silva, J.E. Fluorescent sensor for Cr(VI) based in functionalized silicon quantum dots with dendrimers. *Talanta* **2015**, *144*, 862–867. [[CrossRef](#)]
41. Fernandes, T.; Fateixa, S.; Nogueira, H.I.S.; Daniel-Da-Silva, A.L.; Trindade, T. Dendrimer-Based Gold Nanostructures for SERS Detection of Pesticides in Water. *Eur. J. Inorg. Chem.* **2019**, *2020*, 1153–1162. [[CrossRef](#)]

42. Serenko, O.; Skupov, K.; Bakirov, A.; Kuchkina, N.; Shifrina, Z.; Muzafarov, A. Porosity of Rigid Dendrimers in Bulk: Interdendrimer Interactions and Functionality as Key Factors. *Nanomaterials* **2021**, *11*, 2600. [[CrossRef](#)] [[PubMed](#)]
43. Algarra, M.; Campos, B.B.; Alonso, B.; Casado, C.M.; Da Silva, J.C.E.; Benavente, J. Inclusion of thiol DAB dendrimer/CdSe quantum dots based in a membrane structure: Surface and bulk membrane modification. *Electrochim. Acta* **2013**, *89*, 652–659. [[CrossRef](#)]
44. Connolly, S.; Rao, S.N.; Fitzmaurice, D. Characterization of Protein Aggregated Gold Nanocrystals. *J. Phys. Chem. B* **2000**, *104*, 4765–4776. [[CrossRef](#)]
45. Briggs, D.; Seah, M.P. *Practical Surface Analysis by Auger and X-ray Photoelectron Spectroscopy*; John Wiley & Sons: Chichester, UK, 1995; Volume I.
46. Tompkins, H.G.; McGahan, W.A. *Spectroscopic Ellipsometry and Reflectometry: A User's Guide*; Wiley: Hoboken, NJ, USA, 1999; ISBN 978-0-471-18172-9.
47. Ogieglo, W.; Wormeester, H.; Wessling, M.; Benes, N.E. Spectroscopic Ellipsometry Analysis of a Thin Film Composite Membrane Consisting of Polysulfone on a Porous  $\alpha$ -Alumina Support. *ACS Appl. Mater. Interfaces* **2012**, *4*, 935–943. [[CrossRef](#)] [[PubMed](#)]
48. Cuevas, A.L.; Yuso, M.D.V.M.D.; Vega, V.; González, A.S.; Prida, V.M.; Benavente, J. Influence of ALD Coating Layers on the Optical Properties of Nanoporous Alumina-Based Structures. *Coatings* **2019**, *9*, 43. [[CrossRef](#)]
49. Losurdo, M.; Bergmair, M.; Bruno, G.; Cattelan, D.; Cobet, C.; de Martino, A.; Fleischer, K.; Dohcevic-Mitrovic, Z.; Esser, N.; Galliet, M.; et al. Spectroscopic ellipsometry and polarimetry for materials and systems analysis at the nanometer scale: State-of-the-art, potential, and perspectives. *J. Nanopart. Res.* **2009**, *11*, 1521–1554. [[CrossRef](#)] [[PubMed](#)]
50. Logothetidis, S.; Gioti, M.; Gravalidis, C. Optical and electronic characterization on polymeric membranes. *Synth. Met.* **2003**, *138*, 369–374. [[CrossRef](#)]
51. Vera, R.; Gelde, L.; Antico, E.; de Yuso, M.M.; Benavente, J.; Fontas, C. Tuning physicochemical, electrochemical and transport characteristics of polymer inclusion membrane by varying the counter-anion of the ionic liquid Aliquat 336. *J. Membr. Sci.* **2017**, *529*, 87–94. [[CrossRef](#)]
52. Macdonald, J.R.; Johnson, W.B. Fundamentals of Impedance Spectroscopy. In *Impedance Spectroscopy: Theory, Experiment, and Applications*, 3rd ed.; Barsoukov, E., Ed.; Wiley Online Library: New York, NY, USA, 2018. [[CrossRef](#)]
53. Fortunato, R.; Branco, L.C.; Afonso, C.A.M.; Benavente, J.; Crespo, J.G. Electrical impedance spectroscopy characterisation of supported ionic liquid membranes. *J. Membr. Sci.* **2006**, *270*, 42–49. [[CrossRef](#)]
54. Vázquez, M.; Romero, V.; Fontas, C.; Antico, E.; Benavente, J. Polymer inclusion membranes (PIMs) with the ionic liquid (IL) Aliquat 336 as extractant: Effect of base polymer and IL concentration on their physical–chemical and elastic characteristics. *J. Membr. Sci.* **2014**, *455*, 312–319. [[CrossRef](#)]
55. Moulder, J.F.; Stickle, W.; Sobol, P.; Bomben, K.D. *Handbook of X Ray Photoelectron Spectroscopy: A Reference Book of Standard Spectra for Identification and Interpretation of XPS Data*; Physical Electronics: Eden Prairie, MN, USA, 1995.
56. Zhao, M.; Cao, Y.; Liu, X.; Deng, J.; Li, D.; Gu, H. Effect of nitrogen atomic percentage on N<sup>+</sup>-bombarded MWCNTs in cytocompatibility and hemocompatibility. *Nanoscale Res. Lett.* **2014**, *9*, 142. [[CrossRef](#)]
57. Benavente, J. Use of impedance spectroscopy for characterization of membranes and the effect of different modifications. In *Membrane Modification: Technology and Applications*; Hilal, N., Khayet, M., Wright, C.J., Eds.; CRC Press: Boca Raton, FL, USA, 2012.
58. Gelde, L.; Cuevas, A.L.; Benavente, J. Influence of Pore-Size/Porosity on Ion Transport and Static BSA Fouling for TiO<sub>2</sub>-Covered Nanoporous Alumina Membranes. *Appl. Sci.* **2021**, *11*, 5687. [[CrossRef](#)]
59. Rene-Boisneuf, L.; Scaiano, J.C. Sensitivity versus Stability: Making Quantum Dots More Luminescent by Sulfur Photocuring without Compromising Sensor Response. *Chem. Mater.* **2008**, *20*, 6638–6642. [[CrossRef](#)]
60. Available online: [www.vaxasoftware.com](http://www.vaxasoftware.com) (accessed on 10 December 2021).
61. Hamizi, N.A.; Johan, M.R. Optical Properties of CdSe Quantum Dots via Non-TOP based Route. *Int. J. Electrochem. Sci.* **2012**, *7*, 8458–8467.